PHYSICS OF FLUIDS **27**, 012001 (2015)

A general flux-based analysis for spherical electrocatalytic nanomotors

Amir Nourhani,[1,2,a)] Paul E. Lammert,[1] Vincent H. Crespi,[1,3,4] and Ali Borhan[2]
[1]*Department of Physics, The Pennsylvania State University, University Park, Pennsylvania 16802, USA*
[2]*Department of Chemical Engineering, The Pennsylvania State University, University Park, Pennsylvania 16802, USA*
[3]*Department of Materials Science and Engineering, The Pennsylvania State University, University Park, Pennsylvania 16802, USA*
[4]*Department of Chemistry, The Pennsylvania State University, University Park, Pennsylvania 16802, USA*

(Received 15 July 2014; accepted 5 December 2014; published online 6 January 2015)

We present a flux-based analysis of the motion of spherical electrocatalytic nanomotors based on an electrokinetic model with general distribution of cation flux over the motor surface. Using the method of matched asymptotic expansions, we find a general expression for the motor velocity to leading order in the Debye length in the limit of weak surface cation flux. The nanomotor velocity is proportional to the first Legendre coefficient of surface cation flux and depends non-linearly on the interfacial potential at the particle surface, inversely on the fluid viscosity and background ion concentration in the electrolyte. The results are consistent with previous experimental observations and numerical calculations. We also provide a scaling analysis that portrays the physical picture of self-electrophoresis at the molecular level based on migration of ions and transfer of their momentum to fluid. © *2015 AIP Publishing LLC*. [http://dx.doi.org/10.1063/1.4904951]

I. INTRODUCTION

The development of artificial nanomotors during the past decade has created a fascinating new area in colloid science focused on powered motion at the nanoscale.[1–14] Self-locomotion at low Reynolds number has been studied for many years in biological systems.[15–19] New artificial nanomotors exhibit linear[20–26] and rotational motion[27–36] in abiotic systems without external driving forces. To assist experimental efforts in developing faster[22–24] and more functional[37,38] nanomotors, mathematical models of motor function[39–44] have been developed to relate the velocity and performance of motors to the physical parameters of the nanomotor and its environment. The proposed motion mechanisms include self-diffusiophoresis,[41,42] self-thermophoresis,[45–49] self-acoustophoresis,[50,51] bubble propulsion,[51–55] osmotic propulsion,[56,57] and self-electrophoresis.[58–65]

The concept of self-electrophoretic propulsion dates back to Mitchell,[66,67] who suggested it as a mechanism for micro-organism motion. Lammert *et al.*[39] made a quantitative model and suggested that it might apply to cyanobacteria, though that proposal was shown untenable[68] due to the high salinity of their environment. To date, self-electrophoresis has not been demonstrated in living systems, but it has recently been realized in synthetic inorganic systems. Paxton *et al.*[20] fabricated half-gold/half-platinum (Au/Pt) bimetallic rods approximately 2 μm long and 370 nm in diameter, which move autonomously with speeds of 10-20 μm/s in aqueous solutions of a few percent hydrogen peroxide. Kline *et al.*[37] fabricated five segment Pt/Ni/Au/Ni/Au motors to control

a)Electronic mail: nourhani@psu.edu

the direction of motion by means of an external magnetic field, and Burdick *et al.*[69] synthesized Au/Ni/Au/Pt-CNT nanomotors and magnetically sorted them into microchannels.

The autonomous powered motion of these electrocatalytic nanomotors has been ascribed to electrokinetic self-propulsion.[58–65] The connected metals in hydrogen peroxide solution comprise a mobile electrochemical cell.[58] The overall catalytic reaction is achieved through the anodic oxidation of hydrogen peroxide, which produces hydrogen ions, and the cathodic reduction of hydrogen peroxide, which consumes hydrogen ions, possibly supplemented by reduction of oxygen. The anodic reaction is predominant on the platinum surface and the cathodic reaction on the gold surface, so that a current of hydrogen ions is forced to flow from one side to the other. Wang *et al.*[58] measured speeds and direction of motion for bimetallic rods composed of almost all possible pairs of Rh, Pt, Ni, Pd, Au, and Ru. The results agreed with expectations based on classic electrochemical measurements of currents through microelectrodes of those metals connected to a standard electrode through an external bias, strongly supporting the hypothesis that the motive mechanism is electrokinetic.

Having established the electrokinetic self-propulsion mechanism experimentally, more insight into different aspects of the phenomenon can be obtained by theoretically studying a set of governing equations that describe the motion of ions in the electrolyte, the relation between the electric potential and the local ion concentration, and the fluid flow mediated by an electric body force. Such a framework has been used extensively to address the electrophoretic motion of colloidal dielectrics and metals subjected to an external driving force in an electrolyte.[70–78] In the case of electrocatalytic nanomotors, the driving forces are not external but generated through the action of electrochemical processes on the surface of the motor. Therefore, any electrokinetic model for such swimmers must include appropriate boundary conditions that address electrochemical production and consumption of hydrogen ions over the surface of the nanomotor. Two different approaches have been pursued in the literature; a flux-based approach and a kinetics-based approach.

In the *flux-based* approach, we simply posit an *ad hoc* pattern of ion flux over the surface of the particle and apply the governing equations mentioned above. This approach has been successfully applied numerically by Moran *et al.*,[60] who assumed a piecewise-uniform surface flux of hydrogen ions to obtain motor velocities in the range of experimental observations. Later, using a similar approach, Wang *et al.*[61] obtained a power conversion efficiency of order 10^{-9} for Pt/Au nanorods, in agreement with estimates based on their experimental data.

The *kinetics-based* approach, on the other hand, folds in electrochemical reaction kinetics on the nanomotor surface from the very beginning.[62–65] Yariv[62] analytically solved a general redox model (linear in cation concentration C_+) for the velocity of conductive spherical and slender-body nanomotors in a symmetric binary electrolyte in the limit of thin electrical double layer and weak variation of the kinetic coefficients over the nanomotor surface. A more system-specific approach to address the decomposition of hydrogen peroxide on bimetallic nanomotors using redox kinetics was pursued numerically by Moran and Posner (second order in C_+) for cylindrical motors,[63,64] and both numerically and analytically by Sabass and Seifert (first order in C_+) for spherical motors.[65]

Both approaches successfully address experimental observations. The kinetics-based route is less *ad hoc* than the flux-based method, but uncertainty about surface properties and the individual reaction steps involved in the catalysis complicates its application. When the reaction kinetics is either too complicated or unknown, an empirical flux-based approach seems the only option and has yielded good predictions.[60,61] While the kinetics-based approach has been studied both numerically[63–65] and analytically,[62,65] the flux-based approach has been used only numerically[60,61] for the special case of a piecewise-uniform surface distribution of cation flux.

In this paper, we fill this gap by obtaining an analytical solution based on a general flux-based boundary condition, and giving a qualitative analysis from a molecular perspective that explains the scaling of motor speed with all the relevant parameters. A flux-based model is set up in Sec. II, consisting of a set of governing equations similar to those used in previous studies[60–65] combined with problem-specific boundary conditions. We assume a general surface distribution for cation flux which can be assigned a specific form such as a piecewise-uniform flux,[60,61] or given a more complicated *ad hoc* distribution to address the multimetallic nanomotors of Kline *et al.*[37] and Burdick *et al.*[69] Alternatively, the surface cation flux distribution can be calculated by requiring

consistency with a given redox kinetics to connect flux-based and kinetics-based approaches (Appendix A). Section III contains the analytical solution of this model in the limit of thin diffuse layer to linear order in surface flux. Section IV provides a new scaling analysis that captures the essential physics of self-electrophoretic motion using elementary physical reasoning. Section V defines surface cation flux efficiency and elucidates the general effects of surface cation flux distribution on the performance of a motor. For the reader who is disinclined to wade through the formalism of Secs. II and III, we suggest reading Sec. II up through Eq. (5) for notational familiarity, consulting Eq. (35), and then proceeding directly to Secs. IV and V, which are independent of the formal apparatus.

II. PROBLEM FORMULATION

We model the nanomotor and its environment as a conductive spherical particle moving under isothermal conditions in a symmetric binary electrolyte of cations (+) and anions (−) with ionic valences z_+ and z_- ($z_+ = -z_- \equiv z$) and diffusion coefficients D_+ and D_-, respectively. We define $D_{\min} = \min(D_+, D_-)$ as the smallest diffusivity of ions in the electrolyte. The conductive sphere, comprising at least two different catalytic metals in an axisymmetric configuration (see Fig. 1), produces and consumes cations asymmetrically on its surface. We work in the experimentally relevant regime[62,65] where the sphere radius a is much larger than the Debye length

$$\lambda_D \equiv \sqrt{\frac{\epsilon \phi_T}{2zFC_+^\infty}}. \tag{1}$$

Here, ϵ is the permittivity of the fluid, $\phi_T = RT/(zF)$ is the thermal potential, R is the universal gas constant, T is the absolute temperature, F is Faraday's constant, and C_+^∞ is the bulk cation concentration. We write dimensional variables without undertilde (e.g., G) and dimensionless variables with an undertilde (e.g., $\underset{\sim}{G}$). Lengths are made dimensionless with the nanomotor radius a, concentrations with the far-field cation concentration C_+^∞, fluxes with $D_{\min}C_+^\infty/a$, electric potential with the thermal potential $\phi_T = RT/(zF)$, pressure with $\epsilon\phi_T^2/a^2$, and velocity with $\epsilon\phi_T^2/\mu a$, where μ is the fluid viscosity.

The nanomotor surface is impermeable to anions, leading to the boundary condition

$$\hat{n} \cdot \underset{\sim}{\boldsymbol{J}}_-\Big|_{\underset{\sim}{r}=1} = 0 \tag{2}$$

for the surface flux $\underset{\sim}{\boldsymbol{J}}_-$ of negative ions. The surface flux of cations $\hat{n} \cdot \underset{\sim}{\boldsymbol{J}}_+$, on the other hand, is non-zero and asymmetrically distributed over the surface of the nanomotor, with the average

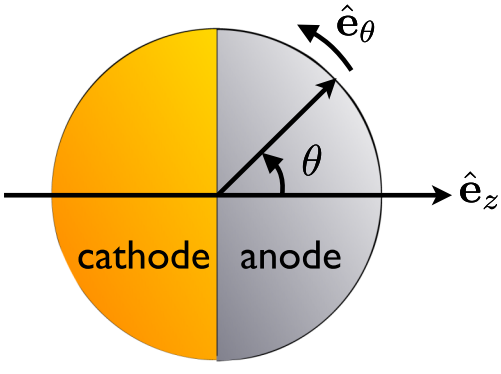

FIG. 1. The nanomotor is modeled as an axisymmetric conductive spherical particle. A general position-dependent flux of hydrogen ions at the surface of the sphere is represented by $\hat{n} \cdot \boldsymbol{J}_+$ which can either be a kinetics-based or an *ad hoc* model-based function. The nanomotor moves with its anode forward.

absolute cation flux on the surface defined as

$$\underset{\sim}{j}_{+} = \frac{\int_{\underset{\sim}{S}} |\hat{n} \cdot \underset{\sim}{\boldsymbol{J}}_{+}| d\underset{\sim}{S}}{\int_{\underset{\sim}{S}} d\underset{\sim}{S}} = \frac{1}{4\pi} \int_{\underset{\sim}{S}} |\hat{n} \cdot \underset{\sim}{\boldsymbol{J}}_{+}| d\underset{\sim}{S}. \tag{3}$$

We write the surface cation flux distribution in the form

$$\hat{n} \cdot \underset{\sim}{\boldsymbol{J}}_{+}\Big|_{\underset{\sim}{r}=1} = \underset{\sim}{j}_{+} f(\theta), \tag{4}$$

where the function $f(\theta) \sim O(1)$ is defined solely for mathematical convenience and does not place any restrictions on our general treatment of the surface cation flux. At steady state, the rates of production and consumption of cations are equal, leading to the constraint

$$\int_{S} \hat{n} \cdot \underset{\sim}{\boldsymbol{J}}_{+} \, dS \propto \int_{0}^{\pi} f(\theta) \, \sin\theta \, d\theta = 0 \tag{5}$$

on the surface cation flux distribution. The ionic fluxes $\underset{\sim}{\boldsymbol{J}}_{\pm}$ in the electrolyte are governed by species conservation equations

$$\underset{\sim}{\nabla} \cdot \underset{\sim}{\boldsymbol{J}}_{\pm} + Pe \, \underset{\sim}{\boldsymbol{U}} \cdot \underset{\sim}{\nabla} \underset{\sim}{C}_{\pm} = 0, \tag{6}$$

where $\underset{\sim}{\boldsymbol{U}}$ is the local fluid velocity, $\underset{\sim}{C}_{\pm}$ denote the local ion concentrations ($\underset{\sim}{C}_{+}$ for cations and $\underset{\sim}{C}_{-}$ for anions), and the Péclet number $Pe \equiv \epsilon \phi_T^2/(\mu D_{\min})$ is the ratio of the characteristic time of slowest ion diffusion to that of convection.

In the dilute regime, the ionic fluxes are related to local ion concentrations and electric potential $\underset{\sim}{\Phi}$ by

$$\underset{\sim}{\boldsymbol{J}}_{\pm} = -\underset{\sim}{\mathcal{D}}_{\pm}(\underset{\sim}{\nabla} \underset{\sim}{C}_{\pm} \pm \underset{\sim}{C}_{\pm} \underset{\sim}{\nabla} \underset{\sim}{\Phi}), \tag{7}$$

where $\underset{\sim}{\mathcal{D}}_{\pm} = D_{\pm}/D_{\min}$. Far from the nanomotor, the electro-neutrality condition in the electrolyte leads to

$$\underset{\sim}{C}_{\pm}(\underset{\sim}{r} \to \infty) = \underset{\sim}{C}_{+}^{\infty} = 1, \tag{8}$$

where $\underset{\sim}{C}_{+}^{\infty}$ is the dimensionless bulk cation concentration. Around the particle, however, an asymmetric cloud of ions is formed with the local ion concentrations related to the local electric potential according to the Poisson equation

$$2\underset{\sim}{\lambda}^2 \underset{\sim}{\nabla}^2 \underset{\sim}{\Phi} = -(\underset{\sim}{C}_{+} - \underset{\sim}{C}_{-}), \tag{9}$$

where $\underset{\sim}{\lambda} = \lambda_D/a$ is the dimensionless Debye length. The electric potential on the equipotential surface of the conductive nanomotor is

$$\underset{\sim}{\Phi}(\underset{\sim}{r} = 1) = \underset{\sim}{\phi} \tag{10}$$

and vanishes far away from the particle, i.e.,

$$\underset{\sim}{\Phi}(\underset{\sim}{r} \to \infty) = 0. \tag{11}$$

The resulting local electric field acts on the ions and consequently exerts a force on the fluid elements containing net charge, thereby generating flow of fluid around the nanomotor. Because of the small size and velocity of the nanomotor, the resulting flow typically has low Reynolds number and is governed by the Stokes and continuity equations, which are written in dimensionless form as

$$\underset{\sim}{\nabla}^2 \underset{\sim}{\boldsymbol{U}} + \underset{\sim}{\nabla}^2 \underset{\sim}{\Phi} \underset{\sim}{\nabla} \underset{\sim}{\Phi} = \underset{\sim}{\nabla} \underset{\sim}{P}, \tag{12a}$$

$$\underset{\sim}{\nabla} \cdot \underset{\sim}{\boldsymbol{U}} = 0, \tag{12b}$$

where $\underset{\sim}{P}$ is the pressure. The second term on the left-hand side of Eq. (12a) represents the body force exerted on the fluid by the local electric field. In the laboratory-fixed frame of reference, the far-field fluid velocity satisfies

$$\underset{\sim}{\boldsymbol{U}}(\underset{\sim}{r} \to \infty) = 0, \tag{13}$$

while the no-slip condition on the surface of the particle requires

$$\underset{\sim}{\boldsymbol{U}}(\underset{\sim}{r} = 1) = \underset{\sim}{\mathcal{U}} \, \hat{\mathbf{e}}_z, \tag{14}$$

where $\underset{\sim}{\mathcal{U}}$ is the nanomotor velocity in the laboratory frame and $\hat{\mathbf{e}}_z$ is a unit vector pointing from cathode to anode parallel to the symmetry axis of the particle, as shown in Fig. 1.

III. NANOMOTOR VELOCITY

Since the dimensionless Debye length is typically small, $\underset{\sim}{\lambda} \ll 1$, the term $\underset{\sim}{\lambda}^2\underset{\sim}{\nabla}^2\underset{\sim}{\Phi}$ in Poisson equation (9) is vanishingly small everywhere in the electrolyte domain except in a thin boundary layer near the surface of the particle where large variations in electric potential occur. Hence, we divide the electrolyte domain into an inner region near the particle surface where the radial change in electric potential is large enough for $\underset{\sim}{\lambda}^2\underset{\sim}{\nabla}^2\underset{\sim}{\Phi}$ to be $O(1)$, and an outer region, where $\underset{\sim}{\lambda}^2\underset{\sim}{\nabla}^2\underset{\sim}{\Phi}$ vanishes to leading order in $\underset{\sim}{\lambda}$. To capture the rapid radial variation of electric potential in the inner region, we stretch the inner region using the transformation $\underset{\sim}{\rho} = (\underset{\sim}{r} - 1)/\underset{\sim}{\lambda}$ and write inner and outer expansions in the form $\underset{\sim}{G}^i(\underset{\sim}{\rho},\theta) = \sum_{k=n_0}^{\infty}\underset{\sim}{\lambda}^k\underset{\sim}{G}^{i(k)}(\underset{\sim}{\rho},\theta)$ and $\underset{\sim}{G}^o(\underset{\sim}{r},\theta) = \sum_{k=0}^{\infty}\underset{\sim}{\lambda}^k\underset{\sim}{G}^{o(k)}(\underset{\sim}{r},\theta)$, respectively, for each field $\underset{\sim}{G}$, where the value of n_0 depends on $\underset{\sim}{G}$.[75] We then match the inner and outer expansions to obtain uniformly valid asymptotic expansions over the entire domain. Since our analysis for the inner region overlaps with Yariv's kinetics-based analysis,[62,75] we briefly review his results in the inner region as Eqs. (15)–(17) and then apply our flux-based analysis for the outer region to obtain the nanomotor velocity.

To leading order in $\underset{\sim}{\lambda}$, in the outer region, the electro-neutrality condition holds,

$$\underset{\sim}{C}_+^{o(0)} = \underset{\sim}{C}_-^{o(0)} \equiv \underset{\sim}{C}^{o(0)}, \tag{15}$$

and the ion concentrations in the inner region obey the local equilibrium condition

$$\underset{\sim}{C}_\pm^{i(0)}(\underset{\sim}{\rho},\theta) = \underset{\sim}{C}^{o(0)}(1,\theta)\,\exp\left(\mp[\underset{\sim}{\Phi}^{i(0)}(\underset{\sim}{\rho},\theta) - \underset{\sim}{\Phi}^{o(0)}(1,\theta)]\right). \tag{16}$$

The slip velocity as the surface boundary condition for the outer region follows:[62,73–75]

$$\underset{\sim}{U}_{slip}^{(0)}(\theta) = \left[\underset{\sim}{\phi}^{(0)} - \underset{\sim}{\Phi}^{o(0)}(1,\theta)\right]\partial_\theta\underset{\sim}{\Phi}^{o(0)}(1,\theta) - 4\frac{\partial_\theta\underset{\sim}{C}^{o(0)}(1,\theta)}{\underset{\sim}{C}^{o(0)}(1,\theta)}\ln\cosh\left[\frac{\underset{\sim}{\phi}^{(0)} - \underset{\sim}{\Phi}^{o(0)}(1,\theta)}{4}\right]. \tag{17}$$

Noting that $\underset{\sim}{J}_{\pm\rho}^{i(-1)} = 0$, the species conservation equations at $O(\underset{\sim}{\lambda}^{-1})$ reduce to $\partial_{\underset{\sim}{\rho}}\underset{\sim}{J}_{\pm\rho}^{i(0)} = 0$, implying that $\underset{\sim}{J}_{\pm\rho}^{i(0)}$ are independent of $\underset{\sim}{\rho}$ in the inner region. Therefore, matching the leading order normal fluxes yields

$$\underset{\sim}{J}_{+r}^{o(0)}(1,\theta) = \underset{\sim}{J}_{+\rho}^{i(0)}(\rho,\theta) = \underset{\sim}{j}_+ f(\theta), \tag{18a}$$

$$\underset{\sim}{J}_{-r}^{o(0)}(1,\theta) = \underset{\sim}{J}_{-\rho}^{i(0)}(\rho,\theta) = 0, \tag{18b}$$

where the leading-order radial fluxes in the outer region are given by

$$\underset{\sim}{J}_{\pm r}^{o(0)} = -\underset{\sim}{\mathcal{D}}_\pm\left[\partial_{\underset{\sim}{r}}\underset{\sim}{C}_\pm^{o(0)} \pm \underset{\sim}{C}_\pm^{o(0)}\partial_{\underset{\sim}{r}}\underset{\sim}{\Phi}^{o(0)}\right]. \tag{19}$$

Using Eq. (7), adding and subtracting the $O(\underset{\sim}{\lambda}^0)$ species conservation equations for positive and negative ions, and using electro-neutrality condition (15), yields

$$\underset{\sim}{\nabla}^2\underset{\sim}{C}^{o(0)} = \left(\frac{\underset{\sim}{\mathcal{D}}_+^{-1} + \underset{\sim}{\mathcal{D}}_-^{-1}}{2}\right)Pe\,\underset{\sim}{\boldsymbol{U}}^{o(0)}\cdot\underset{\sim}{\nabla}\underset{\sim}{C}^{o(0)}, \tag{20a}$$

$$\underset{\sim}{\nabla}\cdot\left(\underset{\sim}{C}^{o(0)}\underset{\sim}{\nabla}\underset{\sim}{\Phi}^{o(0)}\right) = \left(\frac{\underset{\sim}{\mathcal{D}}_+^{-1} - \underset{\sim}{\mathcal{D}}_-^{-1}}{2}\right)Pe\,\underset{\sim}{\boldsymbol{U}}^{o(0)}\cdot\underset{\sim}{\nabla}\underset{\sim}{C}^{o(0)}. \tag{20b}$$

Repeating the same procedure with Eq. (18) and using Eqs. (8), (11), and (19) gives the surface and far-field boundary conditions

$$\partial_{\underset{\sim}{r}}\underset{\sim}{C}^{o(0)} = \underset{\sim}{C}^{o(0)}\partial_{\underset{\sim}{r}}\underset{\sim}{\Phi}^{o(0)} = -\frac{1}{2}\underset{\sim}{\mathcal{D}}_+^{-1}\underset{\sim}{j}_+ f(\theta)\ \text{ as }\ r \to 1, \tag{21a}$$

$$\partial_{\underset{\sim}{r}}\underset{\sim}{C}^{o(0)} = \underset{\sim}{C}^{o(0)}\partial_{\underset{\sim}{r}}\underset{\sim}{\Phi}^{o(0)} = 0 \qquad \text{as } \underset{\sim}{r} \to \infty. \tag{21b}$$

To determine the nanomotor velocity to leading order in $\underset{\sim}{\lambda}$, we need to solve the continuity and Stokes equations at $O(\underset{\sim}{\lambda}^0)$, coupled to Eqs. (20). In the laboratory frame, the leading-order equations

are

$$\nabla^2 \underset{\sim}{U}^{o(0)} + \nabla \Phi^{o(0)} \nabla^2 \Phi^{o(0)} = \nabla P^{o(0)}, \tag{22a}$$

$$\nabla \cdot \underset{\sim}{U}^{o(0)} = 0 \tag{22b}$$

subject to the far-field conditions

$$\underset{\sim}{U}^{o(0)}(r \to \infty, \theta) = 0, \tag{23a}$$

$$P^{o(0)}(r \to \infty, \theta) = 0 \tag{23b}$$

and the surface condition

$$\underset{\sim}{U}^{o(0)}(1, \theta) = \mathcal{U}^{(0)} \hat{\mathbf{e}}_z + U^{(0)}_{slip}(\theta) \hat{\mathbf{e}}_\theta, \tag{24}$$

where $\hat{\mathbf{e}}_\theta$ is a unit vector in the θ direction (see Fig. 1).

To proceed with an analytical solution for nonlinear Eqs. (20)–(22), we linearize them in the weak field limit by using perturbation expansions in the small parameter j_+ as

$$G^{o(0)}(r, \theta) = \sum_{k=0}^{\infty} j_+^k G^{o(0,k)}(r, \theta), \tag{25}$$

where $\phi^{(0,0)} < 0$ is the constant leading-order surface potential, $\Phi^{o(0,0)} = \underset{\sim}{U}^{o(0,0)} = \mathcal{U}^{o(0,0)} = 0$, and $C^{o(0,0)} = C^{\infty}_{+} = 1$. To leading order in j_+, Eqs. (20) and (21) reduce to

$$\nabla^2 G^{o(0,1)} = 0, \tag{26a}$$

$$\partial_r G^{o(0,1)} = -\frac{1}{2} \mathcal{D}_+^{-1} f(\theta) \quad \text{at } r = 1, \tag{26b}$$

$$G^{o(0,1)} = 0 \qquad \text{as } r \to \infty, \tag{26c}$$

where G is either C or Φ. The solution to these equations can be written as

$$C^{o(0,1)}(r, \theta) = \Phi^{o(0,1)}(r, \theta) = \sum_{n=0}^{\infty} \beta_n \frac{\mathrm{P}_n(\cos\theta)}{r^{n+1}}, \tag{27a}$$

$$\beta_n = \frac{2n+1}{4(n+1)} \mathcal{D}_+^{-1} \int_0^{\pi} f(\theta) \mathrm{P}_n(\cos\theta) \sin\theta \, \mathrm{d}\theta \ \text{ for } n \geq 1, \tag{27b}$$

where P_n is the Legendre polynomial of order n. Because of constraint (5), we have $\beta_0 = 0$. To leading order in j_+, boundary conditions (23a) and (24) become

$$\underset{\sim}{U}^{o(0,1)} = \mathcal{U}^{(0,1)} \hat{\mathbf{e}}_z + 4 \ln\left[1 + \tanh(\phi^{(0,0)}/4)\right] \partial_\theta \Phi^{o(0,1)} \hat{\mathbf{e}}_\theta \qquad \text{at } r = 1, \tag{28a}$$

$$\underset{\sim}{U}^{o(0,1)} = 0 \qquad \text{as } r \to \infty, \tag{28b}$$

where we have used $C^{o(0,1)} = \Phi^{o(0,1)}$ in the expansion of the slip velocity (17) in powers of j_+, along with the identity $\ln(1 + \tanh\zeta) = \zeta - \ln\cosh\zeta$. Since the fluid velocity vanishes at far field, we can apply the Lorentz reciprocal theorem[79–81] to obtain

$$\int_S \hat{n} \cdot \underset{\sim}{\mathbb{T}}^{o(0,1)} \cdot \underset{\sim}{U}' \, \mathrm{d}\underset{\sim}{A} = \int_S \hat{n} \cdot \underset{\sim}{\mathbb{T}}' \cdot \underset{\sim}{U}^{o(0,1)} \, \mathrm{d}\underset{\sim}{A}, \tag{29}$$

where the integrals are over the nanomotor surface with outward unit normal $\hat{n}$; $\underset{\sim}{\mathbb{T}}^{o(0,1)}$ is the Newtonian stress tensor corresponding to the flow problem at $O(\lambda^0, j_+)$; and $\underset{\sim}{U}'$ and $\underset{\sim}{\mathbb{T}}'$ are chosen to be the known velocity and stress distributions for the problem of a solid sphere translating with constant speed $\mathcal{U}' = 1$ in the $\hat{\mathbf{e}}_z$ direction in an otherwise quiescent Newtonian fluid at low Reynolds number, for which $\hat{n} \cdot \underset{\sim}{\mathbb{T}}' = -\frac{3}{2}\hat{\mathbf{e}}_z$ everywhere on the particle surface.[79–81] Requiring the particle to be force-free and using Eq. (28a) reduces Eq. (29) to

$$\begin{aligned} \mathcal{U}^{(0,1)} &= 4 \ln\left[1 + \tanh(\phi^{(0,0)}/4)\right] \int_{-1}^{1} \Phi^{o(0,1)}(1, \theta) \cos\theta \, \mathrm{d}(\cos\theta) \\ &= -\frac{8}{3} \beta_1 \ln\left[1 + \tanh(\phi^{(0,0)}/4)\right], \end{aligned} \tag{30}$$

where we have substituted expression (27) for $\tilde{\Phi}^{o(0,1)}(1,\theta)$ and taken advantage of the orthogonality of Legendre polynomials. Thus, to leading order in the dimensionless Debye length $\tilde{\lambda}$ and first order in the dimensionless strength of cation flux $\tilde{j}_+$, the speed of the spherical nanomotor is given by

$$\tilde{\mathcal{U}} = -\frac{8}{3}\beta_1 \tilde{j}_+ \ln\left[1 + \tanh(\tilde{\phi}^{(0,0)}/4)\right] + O(\tilde{\lambda}, \tilde{j}_+^2). \tag{31}$$

As noted, following Eq. (4), we defined the general function $f(\theta) = \tilde{j}_+^{-1}\hat{n}\cdot\tilde{\boldsymbol{J}}_+|_{\tilde{r}=1}$ solely for mathematical convenience and now it is time to eliminate it. Using the first Legendre coefficient $\{\cdot\}_1$ of the surface cation flux

$$\{\hat{n}\cdot\tilde{\boldsymbol{J}}_+|_S\}_1 \equiv \frac{3}{2}\int_{-1}^{1} \hat{n}\cdot\boldsymbol{J}_+|_{\tilde{r}=1}\,\mathrm{P}_1(\cos\theta)\,\mathrm{d}(\cos\theta), \tag{32}$$

and Eqs. (4) and (27), we find

$$\beta_1 \tilde{j}_+ = \frac{1}{4}\tilde{\mathcal{D}}_+^{-1}\{\hat{n}\cdot\tilde{\boldsymbol{J}}_+|_S\}_1 \tag{33}$$

which recasts Eq. (31) into

$$\tilde{\mathcal{U}} \simeq -\frac{2}{3}\{\hat{n}\cdot\tilde{\boldsymbol{J}}_+|_S\}_1\tilde{\mathcal{D}}_+^{-1}\ln\left[1 + \tanh(\tilde{\phi}^{(0,0)}/4)\right]. \tag{34}$$

The dependence of nanomotor velocity on physical parameters such as viscosity, temperature, diffusivity, pH, and charge of ions can be readily identified from the dimensional form of Eq. (34)

$$\mathcal{U} \simeq -\frac{4}{3}\{\hat{n}\cdot\boldsymbol{J}_+\}_1\left(\frac{\lambda_D^2 zF}{\mu D_+}\right)\ln\left[1 + \tanh\frac{\phi^{(0,0)}}{4\phi_T}\right]. \tag{35}$$

Increasing the diffusivity of the cations reduces the asymmetry of the ion cloud, and thus weakens the driving force for fluid motion, resulting in a smaller nanomotor velocity. The diffusivity of anions does not affect the velocity, since there is neither sink nor source of anions on the surface. As expected for low Reynolds number motion, an increase in viscosity increases the drag force and thus reduces the speed of the nanomotor. Temperature effects appear explicitly through ϕ_T and implicitly through other physical parameters such as viscosity or diffusivity.

Expression (35) is general in the sense that for a given surface cation flux distribution and interfacial potential it gives us the nanomotor velocity. What remains is to determine these two quantities. As discussed in the introduction, there are two main approaches for determining $\hat{n}\cdot\boldsymbol{J}_+$ and $\phi^{(0,0)}$. In the flux-based approach,[60,61] these quantities are treated as given, mostly from experimental measurements of j_+[59] and $\phi^{(0,0)}$[82] and *ad hoc* modeling of $f(\theta)$. In the kinetics-based approach, $\hat{n}\cdot\boldsymbol{J}_+$ is related to reactant concentrations through redox kinetics, and $\phi^{(0,0)}$ is obtained from kinetic and physical parameters. To demonstrate the utility of Eqs. (34) and (35) in bridging the kinetics-based and flux-based approaches, Appendix A shows how a redox kinetics model can be incorporated within the framework of our analysis.

IV. PHYSICAL PICTURE

Here, we give a mathematically unencumbered rationalization of the dependence of the motor velocity on physical parameters. Since $j_+ \propto \{\hat{n}\cdot\boldsymbol{J}_+\}_1$ and in the limit $|\phi^{(0,0)}| \ll \phi_T$, $\ln[1 + \tanh(\phi^{(0,0)}/4\phi_T)] \simeq \phi^{(0,0)}/4\phi_T$, Eq. (35) shows the scaling behavior

$$\mathcal{U} \propto \frac{\lambda_D^2 zF}{\mu D_+}|\phi^{(0,0)}|\, j_+. \tag{36}$$

The unpowered motor (i.e., in absence of fuel) has a small but nonzero native charge[82] and a screening cloud of cations around it which falls off exponentially over the Debye length $\lambda_D \ll a$. In the regime of Eq. (36), the screening cloud is just a slight perturbation of the ionic concentrations in the ambient fluid, assumed small enough that we can linearize the ionic concentrations in terms of the dimensionless surface potential $|\phi^{(0,0)}|/\phi_T$. Outside of the diffuse layer, charge-neutrality

holds. Within the diffuse layer, however, the cation concentration is increased and the anion concentration decreased by an amount proportional to $|\phi^{(0,0)}|/\phi_T$ times the bulk cation concentration, as follows from linearizing the Boltzmann factors. Therefore, we have "excess" cation concentration (compared to that of the electro-neutrality condition)

$$C_{+,0}^{\mathrm{exc}} \propto C_{+}^{\infty} \frac{|\phi^{(0,0)}|}{\phi_T} \tag{37}$$

and an electric field

$$\boldsymbol{E}_0 \propto \frac{\phi^{(0,0)}}{\lambda_D} \hat{n} \tag{38}$$

normal to the surface within the diffuse layer around the unpowered motor.

Now, we turn on the motor by adding fuel to the fluid. The motor moves relative to the surrounding fluid. If we immobilize it by a force $\boldsymbol{F}_{\mathrm{ext}}$ external to the system (motor and fluid), then the motor acts as a pump. Upon release of the external force, the motor begins to move, rapidly reaching a steady velocity and experiencing a drag force equal to $\boldsymbol{F}_{\mathrm{ext}}$. For a sphere, Stokes' formula relates the force magnitude to the particle speed

$$\mathcal{U} = -F_{\mathrm{ext}}/(6\pi\mu a). \tag{39}$$

In an unbounded fluid domain, $\boldsymbol{F}_{\mathrm{ext}}$ is the net external force on the system in steady operation of the pump. Hence, $\boldsymbol{F}_{\mathrm{ext}}$ is the net rate at which momentum is added to the system. As the fluid velocity is at steady state, this momentum is evidently not building up anywhere, hence, it must be transported to infinity. Thus, motor speed (39) can be determined by finding the rate of transport of momentum to infinity by the pump. For a confined system, "infinity" means the walls of the container. In the presence of nearby walls, Eq. (39) requires corrections in powers of the ratio of the motor radius to distance of the motor center from the wall.[81] But our arguments should remain qualitatively valid in that case.

The perturbed electrostatic field around a working pump acts on ions and locally injects momentum into the fluid. The charges responsible for this perturbed electrostatic field are both inside the pump and in the fluid. Those inside the pump are partially due to the requirement that the metallic motor body be (nearly) an equipotential. Hence, the perturbation presented to the system of ions-in-solution can equally well be viewed as a static surface charge distribution and cation current at the motor surface, with the *linear* response of the system being the sum of its response to these two perturbations separately. The *static* surface charge distribution evokes a *static* response, with electrostatic body forces balanced by pressure gradients. For our purposes, this can simply be ignored. The flux perturbation creates and maintains an asymmetry in excess cation concentration

$$C_{+}^{\mathrm{exc}} = C_{+,0}^{\mathrm{exc}} + \delta C_{+}^{\mathrm{exc}} \tag{40}$$

with regions of lesser (greater) excess cation concentration near the anode (cathode). This non-equilibrium charge distribution creates a roughly dipolar electric field around the particle which falls off in strength over a distance scaling with the particle size a. Thus, significant current flows throughout a region extending away from the particle surface up to a distance scaling with a. Outside the electrical double layer, charge neutrality holds; cations go in one direction and anions go in the opposite direction, so there is no net momentum transferred to fluid elements. Within the diffuse layer, however, the force on ions due to the effect of the electric field

$$\boldsymbol{E} = \boldsymbol{E}_0 + \delta\boldsymbol{E} \tag{41}$$

on excess cation concentration (40) is, up to first order,

$$C_{+}^{\mathrm{exc}}\boldsymbol{E} \simeq C_{+}^{\mathrm{exc}}\boldsymbol{E}_0 + C_{+,0}^{\mathrm{exc}}\,\delta\boldsymbol{E}. \tag{42}$$

The normal component of the force is compensated by a pressure gradient and only the tangential component of the second term on the right-hand side of Eq. (42) contributes to flow. Therefore, the net momentum transferred into the fluid through electrostatic forces is accounted for by the force on excess cations $C_{+,0}^{\mathrm{exc}}$. We will estimate the momentum transfer through the current due to the motion

of just these excess cations. At steady state, cations are produced at the anode and consumed at the cathode, which requires the motion of excess cations from one side to the other. Cations are produced at a rate $\propto N_A j_+ a^2$ (N_A is Avogadro's number and j_+ is the molar cation flux) and move from anode to cathode in a region extending away from the particle surface up to a distance of scale a, the length scale over which the electric field falls off. Outside the diffuse layer charge neutrality holds, so that forces on cations are compensated by forces on anions, leading to no momentum transfer in that region. Only a fraction equal to the ratio of cross sections $\propto a\lambda_D/a^2 = \lambda_D/a$ passes through the diffuse layer, and out of these cations, only a fraction proportional to $|\phi^{(0,0)}|/\phi_T$ are excess cations and thus responsible for the transfer of momentum. Therefore, the current of excess cations in the diffuse layer is

$$I_{\text{ex}} \propto \left(\frac{|\phi^{(0,0)}|}{\phi_T}\right)\left(\frac{\lambda_D}{a}\right)\left(N_A j_+ a^2\right). \tag{43}$$

As noted earlier, to estimate the rate at which momentum is injected into the fluid, we need only concern ourselves with the force on the excess cations that move within the diffuse layer, since the forces on positive and negative ions outside the diffuse layer are otherwise balanced. We follow a typical ion in excess current (43) along its journey from one side of the motor to the other. Temporarily, let us assume a physical situation where the excess cations are traveling a distance of order a under an electric field in an "unbounded domain" such that the Einstein relation (k_B is Boltzmann's constant)

$$\boldsymbol{v}_{\text{drift}} = \frac{D_+}{k_B T}\boldsymbol{F}_{\text{elec}} \tag{44}$$

relates the cation's drift velocity $\boldsymbol{v}_{\text{drift}}$ to the electrostatic force $\boldsymbol{F}_{\text{elec}}$ on cation. Insofar, as we are considering the ionic current to be dominated by the electrostatic force, this drift velocity can be taken to be the net ion velocity, so that

$$\int \boldsymbol{F}_{\text{elec}}\, dt = \frac{k_B T}{D_+}\int \boldsymbol{v}_{\text{drift}}\, dt = \frac{k_B T}{D_+}\Delta \boldsymbol{X}, \tag{45}$$

where $\Delta \boldsymbol{X}$ is the net displacement of the ion in its journey and $|\Delta \boldsymbol{X}| \propto a$. Then, a typical ion in the imbalance current obtains a net impulse proportional to $ak_B T/D_+$. We obtained this net impulse under the assumption that cations move in an unbounded domain. However, these cations are moving near the nanomotor surface, and their efficiency of momentum transfer to distant fluid is less than 1 because some of the momentum is reabsorbed by the motor through viscous and pressure stresses at the surface: only a portion of this momentum is transferred to infinity (or the walls) through the action of viscosity and pressure. Indeed, the efficiency of this momentum transfer approaches zero as the ion gets closer to the surface, because of the no-slip boundary condition. More precisely (see Appendix B), to leading order in powers of $d/a \ll 1$, d being distance from the surface, the efficiency is proportional to d/a. Since the typical excess cation's average distance from the surface is $\langle d\rangle \propto \lambda_D$, we deduce a momentum transfer efficiency proportional to λ_D/a. Thus, during its trip, an excess cation in the excess current injects net momentum $\sim (ak_B T/D_+)(\lambda_D/a) = \lambda_D k_B T/D_+$ into the distant fluid. Multiplying this momentum by the rate at which ions in the excess current finish their journeys, namely, I_{ex}, we obtain

$$F_{\text{ext}} \propto \left[\frac{k_B T}{D_+}\lambda_D\right]\frac{|\phi^{(0,0)}|}{\phi_T}\frac{\lambda_D}{a}N_A j_+ a^2 = a\frac{Fz\lambda_D^2}{D_+}|\phi^{(0,0)}|\, j_+. \tag{46}$$

Finally, plugging this into Stokes formula (39) recovers scaling speed (36).

V. SURFACE CATION FLUX EFFICIENCY

The analytical character of this general (i.e., not reaction-specific) flux-based approach enables certain insights into the relationship between the surface distribution of cation flux and ultimate motor performance. It is clear from Eq. (34) for the nanomotor velocity that for fixed $\phi^{(0,0)}$ and j_+,

the effects of surface cation flux distribution are encoded in a surface cation flux efficiency η defined as

$$\eta = \frac{\int_0^\pi \hat{n}\cdot\boldsymbol{J}_+ \mathrm{P}_1(\cos\theta)\sin\theta d\theta}{\int_0^\pi |\hat{n}\cdot\boldsymbol{J}_+|\sin\theta d\theta} = \frac{2}{3} j_+^{-1}\{\hat{n}\cdot\boldsymbol{J}_+|_S\}_1. \tag{47}$$

While hydrodynamic efficiency—defined as power output over the sum of hydrodynamic dissipation and power output[83]—deals with the efficiency of a motor's power conversion, the surface cation flux efficiency η measures the optimality of the surface cation flux distribution for a given amount of total electrochemical activity. We would like to know how motor function varies—at fixed j_+ and $\phi^{(0,0)}$—as the distribution of reactivity varies across the surface of the particle. A variety of geometries can be realized by changing the fraction of the particle surface that acts as ion source or sink. For example, Fig. 2 depicts a range of axisymmetric geometries that can be parameterized simply by an angle θ_0. The constraint that the net surface flux of positive ions must be zero at steady state is expressed by Eq. (5), while the total electrochemical reaction rate is measured by $4\pi a^2 j_+$.

In Eq. (47), $|P_1(\cos\theta)|$ is maximum at the poles ($\theta = 0, \pi$) and vanishes at the equator ($\theta = \frac{\pi}{2}$). Thus, η is dominated by the surface cation flux near the poles; what happens near the equator matters little. Therefore, the distinction between a piecewise discontinuous[60,61] distribution and a relatively rapid continuous transition in the cation flux in the vicinity of the equator does not significantly affect η. Consequently, we assume geometries with θ_0 in the general vicinity of the equator and within the empirical flux-based approach, we assume a piecewise-constant surface cation flux distribution of the form

$$\hat{n}\cdot\boldsymbol{J}_+|_S = j_+ \begin{cases} f_+ & \text{if } \theta < \theta_0 \\ -f_- & \text{if } \theta > \theta_0 \end{cases} \tag{48}$$

so that the flux of hydrogen ions is uniform over the source and sink regions. Using Eqs. (3) and (5) yields $f_\pm = 2/(1 \mp \cos\theta_0)$, and we obtain the surface cation flux efficiency $\eta = \frac{1}{2}$, which is the same for all motors in this family, irrespective of the fraction of the surface devoted to source or sink: for fixed total reaction rate, the nanomotor velocity is independent of θ_0. This is consistent with the recent experimental observations of Takagi *et al.*,[84] who reported that varying the Pt/Au ratio from $\frac{1}{3}$ to 3 in their rod-like nanomotors did not significantly affect the motor velocity.

In practical terms, one wishes to maximize motor speed at given fuel concentration, so this result really indicates that θ_0 simply should be tuned to maximize the net electrochemical reaction rate j_+. The more-reactive metal should occupy less area. For θ_0 far from $\frac{\pi}{2}$, the approximation of discontinuous piecewise flux (48) may break down since $\mathrm{P}_1(\cos\theta)$ may be significant in the vicinity of θ_0. If we go beyond the simple source/sink geometry and allow an inert region, it is clear that the surface cation flux distribution efficiency is maximized (at fixed total reaction rate) by limiting the source and sink to small patches at opposite poles. Although η can thus be made to approach unity,

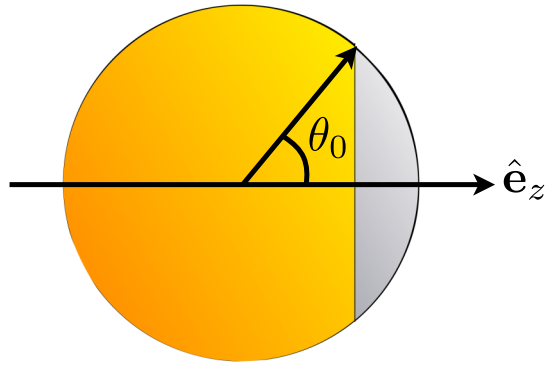

FIG. 2. An axisymmetric spherical bimetallic nanomotor with the surface fraction of each metal parameterized by a single angle θ_0.

such a design would have a small j_+ and, therefore, small speed; at given peroxide concentration, fuel would be used efficiently but could not be consumed rapidly.

VI. CONCLUSION

We have rigorously derived, and given a heuristic explanation of, a general formula (35) for the speed of an electrokinetic motor to leading order in the small Debye length limit and linear in cation flux. It can be applied with an *ad hoc* flux, or consistency can be enforced with a specified chemical kinetics as in Appendix A. The first Legendre coefficient of surface cation flux controls the nanomotor velocity, and a scaling argument provides physical insight into the molecular-level process of momentum transport to infinity that underlies nanomotor operation. In addition to the observations in Sec. V on the surface cation flux efficiency of converting a given amount of electrochemical activity into propulsion, several additional design criteria can be gleaned from our analysis. At least in the linear regime, the charged diffuse layer is the "working fluid" of the motor. Motor speed is increased by charging it more via increased interfacial potential, or by moving it further from the surface via increased Debye length. Thus, manipulating the surface charge of an electrokinetic motor can be useful. At large Debye length, our analysis becomes quantitatively unreliable, though qualitative trends should still be correct. The dependence on Debye length indicates that electrokinetic motors will not perform well at high ionic strength, at least in the linear regime. That is, in their nature, there are some environments to which they are not suited, others to which they are.

ACKNOWLEDGMENTS

This work was supported by the NSF under Grant No. DMR-0820404 through the Penn State Center for Nanoscale Science.

APPENDIX A: REDOX KINETICS

In this section, we calculate $\{\hat{n}\cdot\boldsymbol{J}_+|_S\}_1$ and $\phi^{(0,0)}$ for linear redox kinetics

$$\hat{n}\cdot\boldsymbol{J}_+ = k\left[1 - C_+ / C_+^{\mathrm{Ref}}\right] \tag{A1}$$

which models the net dissolution rate of cations at the nanomotor surface. Here, k represents an effective anodic rate, C_+ is the cation concentration in the liquid adjacent to the nanomotor surface, and C_+^{Ref} is a reference cation concentration that varies over the surface. C_+^{Ref} can be inferred as a fast-kinetic equilibrium concentration, since in the limit $k \to \infty$, the accumulation of cations near the surface would stop cation production.

Yariv[75] neglected the effect of Stern layer in the linear response regime and introduced Eq. (A1) as a first-order Butler-Volmer redox kinetics to study the locomotion of ion-exchange particles in the presence of a weak uniform electric field in the limit of thin diffuse layer. Later, he used the same redox kinetics to solve for the velocity of electrocatalytic nanomotors.[62] In his analysis, the surface variation of the equilibrium cation concentration is modeled by

$$C_+^{\mathrm{Ref}}(\theta) = \langle C_+^{\mathrm{Ref}}\rangle\left[1 + \varepsilon\, C'_+(\theta)\right], \tag{A2}$$

where $\varepsilon \ll 1$ is a small dimensionless parameter and $\langle C_+^{\mathrm{Ref}}\rangle$ represents the surface average of $C_+^{\mathrm{Ref}}(\theta)$ so that $C'_+(\theta)$ satisfies

$$\int_0^\pi C'_+(\theta)\,\sin\theta\, d\theta = 0. \tag{A3}$$

Sabass and Seifert[65] also used a linear Butler-Volmer equation while taking into account a potential drop across the Stern layer. However, the exponential dependence on the position-dependent potential difference is ultimately linearized in their analytical solution and reduced to a constant that can be absorbed in the arbitrary redox kinetic coefficients. As such, the kinetic model used by Sabass and Seifert[65] becomes similar to redox model (A1) used by Yariv.[62,75]

Here, we demonstrate how to connect our flux-based expression (34) to redox kinetics (A1). Cation flux matching condition (18a) in the $O(\tilde{\lambda}^0)$ part of Eq. (A1)'s dimensionless form, combined with radial flux expression (19) and inner region cation distribution (16) yields

$$\phi^{(0)} = \Phi^{o(0)}(1,\theta) + \ln \tilde{C}^{o(0)}(1,\theta) - \ln \tilde{C}_+^{\mathrm{Ref}\,(0)}(\theta) - \ln\left[1 + \frac{\tilde{\mathcal{D}}_+}{Da}\left(\partial_{\tilde{r}}\tilde{C}^{o(0)} + \tilde{C}^{o(0)}\partial_{\tilde{r}}\tilde{\Phi}^{o(0)}\right)\right], \quad \text{(A4)}$$

where the Damkohler number $Da = k\,a/(D_{\min}C_+^{\infty})$ is the ratio of the time scale for diffusion to that for surface reaction. We write the general perturbation form $\tilde{G}^{o(0)} = \tilde{G}^{o(0,0)} + \delta\tilde{G}^{o(0)}$ for each field $\tilde{G}$ to split Eq. (A4) into

$$\tilde{\phi}^{(0,0)} = -\ln \tilde{C}_+^{\mathrm{Ref}\,(0,0)}, \quad \text{(A5a)}$$

$$\delta\tilde{\Phi}^{o(0)} + \delta\tilde{C}^{o(0)} - \frac{\tilde{\mathcal{D}}_+}{Da}\,\partial_{\tilde{r}}\left[\delta\tilde{C}^{o(0)} + \delta\tilde{\Phi}^{o(0)}\right] = \delta\tilde{\phi}^{(0)} + \frac{\delta\tilde{C}_+'^{(0)}}{\tilde{C}_+^{\mathrm{Ref}\,(0,0)}} \qquad \text{at } r = 1. \quad \text{(A5b)}$$

To obtain $\{\hat{n}\cdot\tilde{\boldsymbol{J}}_+|_S\}_1$, we connect the perturbation analyses based on $\tilde{j}_+$ and ε. From $O(\tilde{\lambda}^0)$ reference cation concentration (A2), it follows that $C_+^{\mathrm{Ref}\,(0,0)} = \langle C_+^{\mathrm{Ref}\,(0)}\rangle$ and $\delta\tilde{C}_+^{\mathrm{Ref}\,(0)} = \varepsilon\langle C_+^{\mathrm{Ref}\,(0)}\rangle\tilde{C}_+'^{(0)}(\theta)$. The flux-based perturbation analysis yields $\delta\tilde{\Phi}^{o(0)} = \delta\tilde{C}^{o(0)} = \tilde{j}_+\tilde{\Phi}^{o(0,1)}$ and Eqs. (27) and (33) give $\{\tilde{j}_+\tilde{\Phi}^{o(0,1)}\}_1 = \frac{1}{4}\tilde{\mathcal{D}}_+^{-1}\{\hat{n}\cdot\tilde{\boldsymbol{J}}_+|_S\}_1 r^{-2}$. Using these results in the Legendre expansion of Eq. (A5b) leads to

$$\{\hat{n}\cdot\tilde{\boldsymbol{J}}_+|_S\}_1 = \frac{2\varepsilon\tilde{\mathcal{D}}_+\left\{C_+'^{(0)}\right\}_1}{\left(1 + \frac{2\tilde{\mathcal{D}}_+}{Da}\right)}. \quad \text{(A6)}$$

Substitution of Eqs. (A5a) and (A6) into expression (34), setting $C_+^{\mathrm{Ref}\,(0,0)} = \langle C_+^{\mathrm{Ref}\,(0)}\rangle$, and using the identity $1 + \tanh(\zeta/4) = 2/(1 + \sqrt{e^{-\zeta}})$ recovers Yariv's velocity expression

$$\tilde{\mathcal{U}} \simeq \frac{4}{3}\frac{\varepsilon\{C_+'^{(0)}\}_1}{1 + \frac{2\tilde{\mathcal{D}}_+}{Da}}\ln\left[\frac{1 + \sqrt{\langle C_+^{\mathrm{Ref}\,(0)}\rangle}}{2}\right]. \quad \text{(A7)}$$

Thus, flux-based and kinetics-based methods can be directly connected in the linear response regime.

APPENDIX B: MOMENTUM TRANSFER EFFICIENCY NEAR THE MOTOR SURFACE

In our scaling analysis, we considered the force exerted on ions during their journey from source to sink. At steady state, we have a distribution of point-forces in the fluid resulting from local injection of momentum into the fluid by ions. Consider a tangential point-force $\boldsymbol{F}\delta(\boldsymbol{r} - \boldsymbol{r}_0)$, a distance $d = |r_0| - a$ from a stationary sphere's surface, which results in velocity $\boldsymbol{u}'$ and stress $\mathbb{T}'$ fields in the fluid such that $\nabla\cdot\mathbb{T}' + \boldsymbol{F}\delta(\boldsymbol{r} - \boldsymbol{r}_0) = 0$ at low Reynolds number. We are interested in finding $\boldsymbol{F}_\infty$, the portion of momentum rate $\boldsymbol{F}$ that transfers to infinity (or the walls of the container) by hydrodynamic processes. The remaining portion $\boldsymbol{F}_{\mathrm{mtr}}$ is absorbed by the motor so that $\boldsymbol{F} = \boldsymbol{F}_\infty + \boldsymbol{F}_{\mathrm{mtr}}$. To deal with this problem, first consider a second flow field $(\boldsymbol{u}'', \mathbb{T}'')$ resulting from the motion of a sphere of the same size with velocity $\boldsymbol{\mathcal{V}}$ at low Reynolds number. The Lorentz reciprocal theorem then requires

$$\nabla\cdot(\boldsymbol{u}'\cdot\mathbb{T}'' - \boldsymbol{u}''\cdot\mathbb{T}') = \boldsymbol{u}'\cdot(\nabla\cdot\mathbb{T}'') - \boldsymbol{u}''\cdot(\nabla\cdot\mathbb{T}'). \quad \text{(B1)}$$

Integrating over the fluid domain and using the divergence theorem for the left side-hand results in

$$\boldsymbol{\mathcal{V}}\cdot\boldsymbol{F}_{\mathrm{mtr}} = \boldsymbol{u}''(\boldsymbol{r}_0)\cdot\boldsymbol{F}. \quad \text{(B2)}$$

Hence, for any motor shape in any container, there is a linear relation between the particle velocity $\boldsymbol{\mathcal{V}}$ and the fluid velocity field $\boldsymbol{u}''$, namely,

$$\boldsymbol{u}''(\boldsymbol{r}) = \mathbb{L}(\boldsymbol{r})\cdot\boldsymbol{\mathcal{V}}. \quad \text{(B3)}$$

We will recall the explicit expression for $\mathbb{L}$ for a sphere in unbounded fluid after finishing the general manipulations. Inserting (B3) into (B2) and noting that $\boldsymbol{\mathcal{V}}$ is arbitrary yields

$$\boldsymbol{F}_\infty = \boldsymbol{F} - \boldsymbol{F}_{\text{mtr}} = \left[\mathbb{I} - \mathbb{L}(\boldsymbol{r}_0)^T\right] \cdot \boldsymbol{F}, \tag{B4}$$

where $\mathbb{I}$ is the identity matrix. Now recall that we are interested in $\boldsymbol{r}_0$ very close to the motor surface, and that a no-slip boundary condition holds there so that $\mathbb{L} = \mathbb{I}$ on the surface. Thus, with d denoting distance from the surface, Taylor expansion of $\mathbb{L}^T(\boldsymbol{r})$ about the projection of $\boldsymbol{r}_0$ onto the surface, i.e., $\boldsymbol{r} = \boldsymbol{r}_0^*$, to first order in d leads to

$$\boldsymbol{F}_\infty \approx -d\, \hat{n} \cdot \nabla \mathbb{L}^T\Big|_{\boldsymbol{r}_0^*} \cdot \boldsymbol{F}, \tag{B5}$$

where $\hat{n} \cdot \nabla$ indicates a normal derivative. For a sphere of radius a centered at the origin, the Stokes solution is

$$\mathbb{L} = \mathbb{L}^T = \frac{3a}{4r}\left[\left(1 + \frac{a^2}{3r^2}\right)\mathbb{I} + \left(1 - \frac{a^2}{r^2}\right)\hat{r}\hat{r}\right], \tag{B6}$$

where $r = |\boldsymbol{r}|$, and $\hat{r} = \boldsymbol{r}/r$. Then,

$$\hat{n} \cdot \nabla \mathbb{L}\Big|_{\text{surface}} = \frac{\partial \mathbb{L}}{\partial r}\Big|_{r=a} = -\frac{1}{2a}\mathbb{I} + \frac{3}{2a}\hat{n}\hat{n}, \tag{B7}$$

where $\hat{n}$ is normal to the surface at $\boldsymbol{r}_0^*$. Insofar as we are interested only in $\boldsymbol{F}$ tangent to the surface, the dyadic term $\hat{n}\hat{n}$ does not contribute to $\boldsymbol{F}_\infty$. Therefore, substituting Eq. (B7) into Eq. (B5), we find

$$\boldsymbol{F}_\infty \approx \frac{d}{2a}\boldsymbol{F}, \tag{B8}$$

and the momentum transfer efficiency for a tangential point-force at distance d from the surface is proportional to d/a, as noted in the discussion in the main text following Eq. (45).

[1] W. Wang, W. Duan, S. Ahmed, T. E. Mallouk, and A. Sen, "Small power: Autonomous nano- and micromotors propelled by self-generated gradients," Nano Today **8**, 531 (2013).
[2] G. A. Ozin, "Channel crossing by a catalytic nanomotor," ChemCatChem **5**, 2798 (2013).
[3] W. Gao and J. Wang, "The environmental impact of micro/nanomachines: A review," ACS Nano **8**, 3170 (2014).
[4] S. Sengupta, M. E. Ibele, and A. Sen, "Fantastic voyage: Designing self-powered nanorobots," Angew. Chem., Int. Ed. **51**, 8434 (2012).
[5] T. Mirkovic, N. S. Zacharia, G. D. Scholes, and G. A. Ozin, "Nanolocomotion-catalytic nanomotors and nanorotors," Small **6**, 159 (2010).
[6] S. J. Ebbens and J. R. Howse, "In pursuit of propulsion at the nanoscale," Soft Matter **6**, 726 (2010).
[7] J. Wang and K. M. Manesh, "Motion control at the nanoscale," Small **6**, 338 (2010).
[8] T. Mirkovic, N. S. Zacharia, G. D. Scholes, and G. A. Ozin, "Fuel for thought: Chemically powered nanomotors out-swim nature's flagellated bacteria," ACS Nano **4**, 1782 (2010).
[9] J. Wang, "Can man-made nanomachines compete with nature biomotors?," ACS Nano **3**, 4 (2009).
[10] W. F. Paxton, S. Sundararajan, T. E. Mallouk, and A. Sen, "Chemical locomotion," Angew. Chem., Int. Ed. **45**, 5420 (2006).
[11] H. H. Kung and M. C. Kung, "Catalytic nanomotors-promising leads for new catalytic applications," Appl. Catal., A **309**, 159 (2006).
[12] R. Dreyfus, J. Baudry, M. L. Roper, M. Fermigier, H. A. Stone, and J. Bibette, "Microscopic artificial swimmers," Nature **437**, 862 (2005).
[13] W. F. Paxton, A. Sen, and T. E. Mallouk, "Motility of catalytic nanoparticles through self-generated forces," Chem. - Eur. J. **11**, 6462 (2005).
[14] G. A. Ozin, I. Manners, S. Fournier-Bidoz, and A. Arsenault, "Dream nanomachines," Adv. Mater. **17**, 3011 (2005).
[15] E. M. Purcell, "Life at low Reynolds-number," Am. J. Phys. **45**, 3 (1977).
[16] P. Colinvaux, "Life at low Reynolds-number," Nature **277**, 353 (1979).
[17] C. Dekker and M. G. L. van den Heuvel, "Motor proteins at work for nanotechnology," Science **317**, 333 (2000).
[18] G. Woehlke and M. Schliwa, "Molecular motors," Nature **422**, 759 (2003).
[19] M. L. Yarmush, C. Mavroidis, and A. Dubey, "Molecular machines," Annu. Rev. Biomed. Eng. **6**, 363 (2004).
[20] W. F. Paxton, K. C. Kistler, C. C. Olmeda, A. Sen, S. K. St Angelo, Y. Y. Cao, T. E. Mallouk, P. E. Lammert, and V. H. Crespi, "Catalytic nanomotors: Autonomous movement of striped nanorods," J. Am. Chem. Soc. **126**, 13424 (2004).
[21] P. Dhar, Th. M. Fischer, Y. Wang, T. E. Mallouk, W. F. Paxton, and A. Sen, "Autonomously moving nanorods at a viscous interface," Nano Lett. **6**, 66 (2006).
[22] R. Laocharoensuk, J. Burdick, and J. Wang, "Carbon-nanotuble-induced acceleration of catalytic nanomotors," ACS Nano **2**, 1069 (2008).
[23] U. K. Demirok, R. Laocharoensuk, K. M. Manesh, and J. Wang, "Ultrafast catalytic alloy nanomotors," Angew. Chem., Int. Ed. **47**, 9349 (2008).

[24] N. S. Zacharia, Z. S. Sadeq, and G. A. Ozin, "Enhanced speed of bimetallic nanorod motors by surface roughening," Chem. Commun. **2009**, 5856.
[25] P. M. Wheat, N. A. Marine, J. L. Moran, and J. D. Posner, "Rapid fabrication of bimetallic spherical motors," Langmuir **26**, 13052 (2010).
[26] A. Nourhani, V. H. Crespi, and P. E. Lammert, "Gaussian memory in kinematic matrix theory for self-propellers," Phys. Rev. E **90**, 062304 (2014).
[27] S. Fournier-Bidoz, A. C. Arsenault, I. Manners, and G. A. Ozin, "Synthetic self-propelled nanorotors," Chem. Commun. **2005**, 441.
[28] L. Qin, M. J. Banholzer, X. Xu, L. Huang, and C. A. Mirkin, "Rational design and synthesis of catalytically driven nanorotors," J. Am. Chem. Soc. **129**, 14870 (2007).
[29] Y. Wang, S.-T. Fei, Y.-M. Byun, P. E. Lammert, V. H. Crespi, A. Sen, and T. E. Mallouk, "Dynamic interactions between fast microscale rotors," J. Am. Chem. Soc. **131**, 9926 (2009).
[30] J. G. Gibbs, S. Kothari, D. Saintillan, and Y. P. Zhao, "Geometrically designing the kinematic behavior of catalytic nanomotors," Nano Lett. **11**, 2543 (2011).
[31] J. G. Gibbs and Y.-P. Zhao, "Self-organized multiconstituent catalytic nanomotors," Small **6**, 1656 (2010).
[32] J. G. Gibbs and Y.-P. Zhao, "Design and characterization of rotational multicomponent catalytic nanomotors," Small **5**, 2304 (2009).
[33] L. F. Valadares, Y.-G. Tao, N. S. Zacharia, V. Kitaev, F. Galembeck, R. Kapral, and G. A. Ozin, "Catalytic nanomotors: Self-propelled sphere dimers," Small **6**, 565 (2010).
[34] A. Nourhani, P. E. Lammert, A. Borhan, and V. H. Crespi, "Kinematic matrix theory and universalities in self-propellers and active swimmers," Phys. Rev. E **89**, 062304 (2014).
[35] A. Nourhani, P. E. Lammert, A. Borhan, and V. H. Crespi, "Chiral diffusion of rotary nanomotors," Phys. Rev. E **87**, 050301(R) (2013).
[36] S. Ebbens, R. A. L. Jones, A. J. Ryan, R. Golestanian, and J. R. Howse, "Self-assembled autonomous runners and tumblers," Phys. Rev. E **82**, 015304(R) (2010).
[37] T. R. Kline, W. F. Paxton, T. E. Mallouk, and A. Sen, "Catalytic nanomotors: Remote-controlled autonomous movement of striped metallic nanorods," Angew. Chem., Int. Ed. **44**, 744 (2005).
[38] P. Calvo-Marzal, K. M. Manesh, D. Kagan, S. Balasubramanian, M. Cardona, G.-U. Flechsig, J. Posner, and J. Wang, "Electrochemically-triggered motion of catalytic nanomotors," Chem. Commun. **2009**, 4509.
[39] P. E. Lammert, J. Prost, and R. Bruinsma, "Ion drive for vesicles and cells," J. Theor. Biol. **178**, 387 (1996).
[40] N. B. Saidulu and K. L. Sebastian, "Interfacial tension model for catalytically driven nanorods," J. Chem. Phys. **128**, 074708 (2008).
[41] R. Golestanian, T. B. Liverpool, and A. Ajdari, "Propulsion of a molecular machine by asymmetric distribution of reaction products," Phys. Rev. Lett. **94**, 220801 (2005).
[42] R. Golestanian, "Anomalous diffusion of symmetric and asymmetric active colloids," Phys. Rev. Lett. **102**, 188305 (2009).
[43] R. Golestanian, T. B. Liverpool, and A. Ajdari, "Designing phoretic micro- and nano-swimmers," New J. Phys. **9**, 126 (2007).
[44] A. Nourhani, Y.-M. Byun, P. E. Lammert, A. Borhan, and V. H. Crespi, "Nanomotor mechanisms and motive force distributions from nanorotor trajectories," Phys. Rev. E **88**, 062317 (2013).
[45] H. R. Jiang, N. Yoshinaga, and M. Sano, "Active motion of a janus particle by self-thermophoresis in a defocused laser beam," Phys Rev. Lett. **105**, 268302 (2010).
[46] B. Qian, D. Montiel, A. Bregulla, F. Cichos, and H. Yang, "Harnessing thermal fluctuations for purposeful activities: The manipulation of single micro-swimmers by adaptive photon nudging," Chem. Sci. **4**, 1420 (2013).
[47] L. Baraban, R. Streubel, D. Makarov, L. Han, D. Karnaushenko, O. G. Schmidt, and G. Cuniberti, "Fuel-free locomotion of janus motors: Magnetically induced thermophoresis," ACS Nano **7**, 1360 (2013).
[48] M. Yang and M. Ripoll, "Simulations of thermophoretic nanoswimmers," Phys. Rev. E **84**, 061401 (2011).
[49] R. Golestanian, "Collective behavior of thermally active colloids," Phys. Rev. Lett. **108**, 038303 (2012).
[50] W. Wang, L. A. Castro, M. Hoyos, and T. E. Mallouk, "Autonomous motion of metallic microrods propelled by ultrasound," ACS Nano **6**, 6122 (2012).
[51] D. Kagan, M. J. Benchimol, J. C. Claussen, E. Chuluun-Erdene, S. Esener, and J. Wang, "Acoustic droplet vaporization and propulsion of perfluorocarbon-loaded microbullets for targeted tissue penetration and deformation," Angew. Chem., Int. Ed. **51**, 7519 (2012).
[52] J. G. Gibbs and Y.-P. Zhao, "Autonomously motile catalytic nanomotors by bubble propulsion," Appl. Phys. Lett. **94**, 163104 (2009).
[53] A. A. Solovev, Y. Mei, E. B. Urena, G. Huang, and O. G. Schmidt, "Catalytic microtubular jet engines self-propelled by accumulated gas bubbles," Small **5**, 1688 (2009).
[54] D. A. Wilson, R. J. M. Nolte, and J. C. M. van Hest, "Autonomous movement of platinum-loaded stomatocytes," Nat. Chem. **4**, 268 (2012).
[55] M. Manjare, B. Yang, and Y.-P. Zhao, "Bubble driven quasioscillatory translational motion of catalytic micromotors," Phys. Rev. Lett. **109**, 128305 (2012).
[56] U. M. Córdova-Figueroa and J. F. Brady, "Osmotic propulsion: The osmotic motor," Phys. Rev. Lett. **100**, 158303 (2008).
[57] U. M. Cordova-Figueroa, J. F. Brady, and S. Shklyaev, "Osmotic propulsion of colloidal particles via constant surface flux," Soft Matter **9**, 6382 (2013).
[58] Y. Wang, R. M. Hernandez, D. J. Bartlett, J. M. Bingham, T. R. Kline, A. Sen, and T. E. Mallouk, "Bipolar electrochemical mechanism for the propulsion of catalytic nanomotors in hydrogen peroxide solutions," Langmuir **22**, 10451 (2006).
[59] W. F. Paxton, P. T. Baker, T. R. Kline, Y. Wang, T. E. Mallouk, and A. Sen, "Catalytically induced electrokinetics for motors and micropumps," J. Am. Chem. Soc. **128**, 14881 (2006).
[60] J. Moran, P. Wheat, and J. Posner, "Locomotion of electrocatalytic nanomotors due to reaction induced charge autoelectrophoresis," Phys. Rev. E **81**, 065302(R) (2010).

[61] W. Wang, T.-Y. Chiang, D. Velegol, and T. E. Mallouk, "Understanding the efficiency of autonomous nano- and microscale motors," J. Am. Chem. Soc. **135**, 10557 (2013).
[62] E. Yariv, "Electrokinetic self-propulsion by inhomogeneous surface kinetics," Proc. R. Soc. A **467**, 1645 (2011).
[63] J. L. Moran and J. D. Posner, "Electrokinetic locomotion due to reaction-induced charge auto-electrophoresis," J. Fluid Mech. **680**, 31 (2011).
[64] J. L. Moran and J. D. Posner, "Role of solution conductivity in reaction induced charge auto-electrophoresis," Phys. Fluids **26**, 042001 (2014).
[65] B. Sabass and U. Seifert, "Nonlinear, electrocatalytic swimming in the presence of salt," J. Chem. Phys. **136**, 214507 (2012).
[66] P. Mitchell, "Hypothetical thermokinetic and electrokinetic mechanisms of locomotion in micro-organisms," Proc. R. Phys. Soc. Edinburgh **25**, 32 (1956).
[67] P. Mitchell, "Self-electrophoretic locomotion in microorganisms–bacterial flagella as giant ionophores," FEBS Lett. **28**, 1 (1972).
[68] T. Pitta and H. Berg, "Self-electrophoresis is not the mechanism for motility in swimming cyanobacteria," J. Bacteriol. **177**, 5701 (1995).
[69] J. Burdick, R. Laocharoensuk, P. M. Wheat, J. D. Posner, and J. Wang, "Synthetic nanomotors in microchannel networks: Directional microchip motion and controlled manipulation of cargo," J. Am. Chem. Soc. **130**, 8164 (2008).
[70] D. A. Saville, "Electrokinetics effects with small particles," Annu. Rev. Fluid Mech. **9**, 321 (1977).
[71] V. A. Murtsovkin, "Nonlinear flows near polarized disperse particles," Colloid J. **58**, 341 (1996).
[72] E. Yariv, "Boundary-induced electrophoresis of uncharged conducting particles: Remote wall approximations," Proc. R. Soc. A **465**, 709 (2009).
[73] D. C. Prieve, J. L. Anderson, J. P. Ebel, and M. E. Lowell, "Motion of a particle generated by chemical gradients. Part 2. Electrolytes," J. Fluid Mech. **148**, 247 (1984).
[74] R. A. Rica and M. Z. Bazant, "Electrodiffusiophoresis: Particle motion in electrolytes under direct current," Phys. Fluids **22**, 112109 (2010).
[75] E. Yariv, "Migration of ion-exchange particles driven by a uniform electric field," J. Fluid Mech. **655**, 105 (2010).
[76] O. Schnitzer and E. Yariv, "Induced-charge electro-osmosis beyond weak fields," Phys. Rev. E **86**, 061506 (2012).
[77] Y. Ben, E. A. Demekhin, and H.-C. Chang, "Nonlinear electrokinetics and "superfast" electrophoresis," J. Colloid Interface Sci. **276**, 483 (2004).
[78] B. Zaltzman and I. Rubinstein, "Electro-osmotic slip and electroconvective instability," J. Fluid Mech. **579**, 173 (2007).
[79] J. Happel and H. Brenner, *Low Reynolds Number Hydrodynamics* (Springer, New York, NY, 1983).
[80] L. G. Leal, *Advanced Transport Phenomena: Fluid Mechanics and Convective Transport Processes* (Cambridge University Press, New York, 2007).
[81] S. Kim and S. J. Karrila, *Microhydrodynamics: Principles and Selected Applications* (Dover Publications, 2005).
[82] G. M. Dougherty, K. A. Rose, J. B. H. Tok, S. S. Pannu, F. Y. S. Chuang, M. Y. Sha, G. Chakarova, and S. G. Penn, "The zeta potential of surface - functionalized metallic nanorod particles in aqueous solution," Electrophoresis **29**, 1131 (2008).
[83] B. Sabass and U. Seifert, "Efficiency of surface-driven motion: Nanoswimmers beat microswimmers," Phys. Rev. Lett. **105**, 218103 (2010).
[84] D. Takagi, A. B. Braunschweig, J. Zhang, and M. J. Shelley, "Dispersion of self-propelled rods undergoing fluctuation-driven flips," Phys Rev. Lett. **110**, 038301 (2013).